Fuel Processing Technology 229 (2022) 107182

Contents lists available at ScienceDirect

Fuel Processing Technology

journal homepage: www.elsevier.com/locate/fuproc

Optimization of the performance of bulk NiO catalyst in the oxidative dehydrogenation of ethane by tuning the synthesis parameters

Yousra Abdelbaki [a,b,c], Agustín de Arriba [a], Rachid Issaadi [c], Rita Sánchez-Tovar [b], Benjamín Solsona [b,*], José M. López Nieto [a,*]

[a] Instituto de Tecnología Química, Universitat Politècnica de València-Consejo Superior de Investigaciones Científicas, Avenida de los Naranjos s/n, Valencia, Spain
[b] Departament d'Enginyeria Química, Universitat de València, C/ Dr. Moliner 50, 46100 Burjassot, Valencia, Spain
[c] Hydrogen Energy Applications Laboratory, Faculty of Technology, University of Blida 1, Algeria

ARTICLE INFO

Keywords:
ODH ethane
NiO
Oxalic acid: calcination temperature
Electrophilic oxygen

ABSTRACT

Highly stable and selective bulk NiO catalysts have been synthesized for the oxidative dehydrogenation (ODH) of ethane to ethylene. Interestingly, by optimizing synthesis parameters such as the amount of oxalic acid in the synthesis gel and the calcination temperature, undoped NiO catalysts have shown a consistent selectivity to ethylene of ca. 75%. The optimal catalyst requires the presence of a certain amount of oxalic acid in the synthesis gel and a final calcination at low temperatures (i.e. 350 °C). These catalysts have been deeply characterized by means of XRD, TPR, HRTEM, Raman and UV–vis diffuse reflectance spectroscopies, XPS and Electrochemical Impedance Spectroscopy measurements and tested in the ethane ODH. A novel electrochemical study has been undertaken, showing the p-character of all the NiO catalysts synthesized but differing in their capacitance values and density of cationic vacancies. The catalytic performance of NiO catalysts has been explained in terms of the different physicochemical properties (including changes in the number of vacancies) of the samples and the isolation of electrophilic oxygen species.

1. Introduction

Currently, the industry of ethylene derivatives presents two opposing trends. On the negative side, the storage and disposal of plastics (among which those derived from ethylene are highlighted) is environmentally complicated. On the other hand, the future limitation of oil derivatives and natural gas for their use in the automotive industry and as fuels suggests a great availability of oil and natural gas for conversion into light olefins in the mid-term. Unlike other chemicals, ethylene production has continuously increased even in the economic recession of 2008. In fact, before the corona outbreak, the expected ethylene consumption worldwide for 2021 was higher than 190 million metric tons [1,2], which is ca. 25% more than the consumption in 2011.

Currently, most ethylene is produced via steam cracking of ethane, LPG and naphtha. This process presents several problems [2–5] among which the high energy consumption stands out. To save these drawbacks related to the energy consumption, the oxidative dehydrogenation (ODH) of ethane is a clean alternative worthy to be studied. Moreover, the ODH of ethane requires fewer separation units than steam cracking, uses catalysts which hardly deactivate (due to the in-situ regeneration by the oxygen consumed), and shows negligible coke formation (which reduces the number of by-products) [1,5,6].

The two most promising catalytic systems for the ODH of ethane are multicomponent Mo-V-Te-Nb-O catalysts [7–9] and promoted or supported NiO catalysts [10–16].

Bulk NiO is a p-type semiconductor [17–19] which, when working as a catalyst in the presence of ethane or olefins and oxygen, tends predominantly to the formation of carbon oxides [18,19]. However, by incorporating an appropriate promoter to the NiO (such as Nb^{5+} [11,20–22]) or supporting it with a suitable material such as Al_2O_3 [10,23–26], the ethylene formation can be drastically enhanced. The nature of the support and/or the promoter must be carefully selected, otherwise the amount of ethylene formed can be even lower than that using unpromoted NiO, as this is the case of potassium as promoter [21]. Then, it has been widely reported that the excess of the electrophilic oxygens in undoped NiO can be decreased by using different cations with high valences (such as W^{6+}, Nb^{5+}, Sn^{4+}, Zr^{4+}, Ti^{4+}) and this positively affects the formation of ethylene [17–21,27–32]. Promoters

* Corresponding authors.
E-mail addresses: benjamin.solsona@uv.es (B. Solsona), jmlopez@itq.upv.es (J.M. López Nieto).

https://doi.org/10.1016/j.fuproc.2022.107182
Received 5 October 2021; Received in revised form 19 January 2022; Accepted 20 January 2022
Available online 1 February 2022
0378-3820/© 2022 Elsevier B.V. All rights reserved.

with acidic characteristics [17–21,27–32] or supports like TiO_2 [23], Al_2O_3 [10,34,35] or siliceous porous clay heterostructure [36] favour the ethylene formation. However, the presence of strong Lewis acid sites provokes the decomposition of ethylene resulting in a low selectivity to olefin [1,6,34,37,38]. Therefore, an excess of promoter usually leads to a decrease in the olefin formation. In this way, it has been demonstrated that in promoted NiO catalysts a loss in the conductivity takes place in the catalysts with an enhanced ethylene formation [18,19,39], which could be related to a decrease in the non-stoichiometric oxygen.

On the other hand, the crystallite size of NiO is also a factor that has been shown as crucial in promoted NiO catalysts, those with lower size presenting the highest ethylene formation [11,28,30–32]. This is especially notable in the case of supported NiO catalysts, in which the desired Ni-support interaction involves a decrease in the mean NiO crystallite size [34–36], whereas low Ni-support interaction leads to large NiO crystallites [40,41].

In most of these studies dealing with promoted NiO catalysts, the catalytic results have been explained in terms of the characteristics of NiO and the way the cation employed influences the physicochemical properties of the nickel oxide (NiO crystallite size, amount of non-stoichiometric oxygen, morphology, lattice parameters, conductivity…). However, it seems that most times the possible direct role of the promoter has been underestimated. Then, in order to properly assign the catalytic properties to the nickel species it would be desirable to study pure NiO catalysts instead of supported or promoted NiO catalysts. For example, in Nb-promoted NiO catalysts the formation of a Ni–Nb-O solid solution was identified as the selective sites in the ethane ODH, and maybe the amount of non-stoichiometric oxygen is not so tightly related to the selectivity to ethylene [19]. However, this behaviour can change if promoters, especially Nb^{5+}, are absent (if niobium is not present in the catalyst formulation).

Recently, Zhao et al. [41] studied undoped NiO showing that it is possible to tune the concentration of non-stoichiometric oxygen with low changes in morphology. In that work, using NiO samples calcined at different temperatures the amount of non-stoichiometric oxygen could be modified and, unlike that proposed in promoted NiO catalysts, it was observed that the selectivity to ethylene increased as the amount of that excess of oxygen increased. On the other hand, the particle size has also been proposed as an important parameter in the performance in the ODH of ethane. In this way, mesostructured NiO catalysts seem to present higher selectivity to ethylene (at isoconversion conditions) than the corresponding nanostructured NiO [42].

At the present work, we have synthesized, characterized and tested in the oxidative dehydrogenation of ethane a set of pure NiO catalysts modifying both the concentration of oxalic acid in the synthesis gel and the final calcination temperature. Moreover, we have studied the influence of different parameters such as the nature of Ni-species, the amount of non-stoichiometric oxygen, the NiO crystallite size or the charge carriers' density of the catalysts on the catalytic performance.

2. Experimental

2.1. Catalyst preparation

Nickel oxides catalysts were prepared through the evaporation at 90 °C of aqueous solutions of nickel nitrate (> 99.99% Sigma-Aldrich) with different amount of oxalic acid (> 99.5% Acros Organics) in the synthesis gel. The solids were dried overnight in a furnace at 120 °C and, finally, they were calcined in static air for 2 h at 350 or 500 °C with a heating ramp of 5 °C/min from room temperature to the desired final calcination temperature. The catalysts will be named as **Ni-x-Y**, where x is the oxalic acid/nickel ratio in the synthesis gel (i.e. Oxalic acid/Ni molar ratio of 0, 0.8, 1.0, 1.5 or 3), and Y is the calcination temperature (350 or 500 °C). Nomenclature and physicochemical properties of these catalysts are shown in Table 1.

Table 1
Physicochemical properties of NiO catalysts.

Catalyst	Oxalate/Ni ratio [a]	Lattice parameter by TEM	Mean particle size by XRD (nm)[b]	Surface area ($m^2\ g^{-1}$)	N_A (cm^{-3})[c]
Ni-0-350	0	0.419	11.9	70.7	$1.39{\cdot}10^{22}$
Ni-0.8-350	0.8	n.d.[d]	8.5	110.3	n.d.[d]
Ni-1-350	1.0	0.416	7.0	70.8	$2.50{\cdot}10^{20}$
Ni-1.5-350	1.5	n.d.[d]	7.9	76.1	n.d.[d]
Ni-3-350	3.0	0.416	5.0	74.0	$2.15{\cdot}10^{20}$
Ni-0-500	0	0.417	21.5	11.8	$1.04{\cdot}10^{21}$
Ni-0.8-500	0.8	n.d.[d]	17.5	24.3	n.d.[d]
Ni-1-500	1.0	0.416	17.0	23.3	$2.55{\cdot}10^{20}$
Ni-1.5-500	1.5	n.d.[d]	17.8	19.9	n.d.[d]
Ni-3-500	3.0	0.416	17.4	24.4	$2.02{\cdot}10^{20}$

[a] Oxalic acid/Ni molar ratio in the synthesis gel; [b] Determined by Scherrer equation from Fig. 3; [c] Acceptor density, N_A, calculated from the slope of the linear region of the Mott-Schottky plot (see Fig. 9); [d] n.d. means not determined.

2.2. Catalysts characterization

X-ray diffraction patterns were collected in an Enraf Nonius FR590 diffractometer with a monochromatic $CuK_{\alpha 1}$ source operated at 40 keV and 30 mA. The size of the NiO domains has been calculated through XRD technique by the Scherrer' equation, $D = k{\cdot}\lambda/w{\cdot}\cos\theta$, where D is the crystallite size, k is a shape factor (0.9), λ is the X-ray wavelength (0.15406 nm), w is the full width at half maximum intensity (FWHM, in radians) and Θ is the Bragg angle [43].

The surface area of catalysts were determined by multi-point N_2 adsorption at −196 °C. Estimations of surface areas were made in accordance with the BET method.

Raman spectra were obtained in an inVia Renishaw spectrometer, equipped with an Olympus microscope, using a wavelength of 514 nm (visible Raman) or 325 nm (UV-Raman), generated with a Renishaw HPNIR laser with a power of approximately 15 mW.

UV–vis diffuse reflectance spectroscopy (DRS) measurements of the solids were carried out within the 200–800 nm range using a *Varian* spectrometer model Cary 5000.

Temperature-programmed reduction experiments (H_2-TPR) were carried out in an Autochem 2910 (Micromeritics) equipped with a TCD detector, using 0.10 g of catalyst and a reducing gas of 10% H_2 in Ar (total flow rate of 50 mL min^{-1}). The samples were heated from room temperature to 800 °C, with a heating rate of 10 °C/min.

X-ray photoelectron spectroscopy (XPS) measurements were performed on a SPECS spectrometer equipped with a Phoibos 150 MCD-9 detector using a monochromatic Al Kα (1486.6 eV) X-ray source. Spectra were recorded using an analyzer pass energy of 50 eV, an X-ray power of 100 W, and an operating pressure of 10^{-9} mbar. Spectra treatment was performed using CASA software. Binding energies (BE) were referenced to C *1s* at 284.5 eV.

TEM (transmission electron microscopy), HRTEM (high resolution transmission electron microscopy) and SAED (Selected area electron diffraction) were conducted using a FEI Field Emission gun Tecnai G2 F20 S-TWIN microscope working at 200 kV. Structural and morphological characterizations were obtained from the TEM and HRTEM images. The lattice parameters were determined via Fourier transformation from HRTEM images. The preparation of the samples for the microscopy analyses involves the sonication in ethanol of the sample and a further

deposition of the solution over a holey-carbon film supported on a Cu grid where it is finally dried.

Electrochemical Impedance Spectroscopy measurements (EIS) were performed at a frequency of 5000 Hz in a 0.1 M Na_2SO_4 electrolyte. The potential was scanned from 1 $V_{Ag/AgCl}$ in the negative direction using an amplitude signal of 0.01 V at 0.05 V/s. For this purpose, a three-electrode electrochemical cell was used. The catalyst was the working electrode (deposited on fluorine tin oxide (FTO)), a platinum tip the counter electrode and an Ag/AgCl (3 M KCl) the reference electrode. An area of 0.5 cm^2 of the catalysts was exposed to the electrolyte. From EIS results, Mott-Schottky plots were carried out to evaluate the semiconductor behaviour of the catalysts and to determine their density of dopants.

2.3. Catalytic tests for ethane ODH

The catalytic tests in the oxidative dehydrogenation of ethane were carried out at atmospheric pressure in a tubular isothermal flow quartz reactor (15 mm inner diameter) at 300–340 °C, with a mixture consisting of C_2H_6/O_2/He with a molar ratio of 3/1/29. Ethane (99.95% purity, Carburos Metálicos) and O_2 (99.995% purity, Carburos metálicos) were used in these experiments. Typical reaction conditions used were 0.1-0.5 g of catalyst and 100 mL min^{-1}, although both the total flow and/or the catalyst amounts were changed in order to achieve different ethane conversions. Catalysts were introduced in the reactor diluted with silicon carbide in order to keep a constant volume in the catalytic bed. Reactants and products were analyzed by gas chromatography using two packed columns: (i) molecular sieve 5 Å (2.5 m); and (ii) Porapak Q (3 m). Blank runs were undertaken without catalyst until 450 °C and no conversion was observed in all cases [28].

3. Results

NiO catalysts heat-treated in air at different temperatures (350 or 500 °C) with or without the addition of oxalic acid in the synthesis gel have been prepared, tested in the oxidative dehydrogenation of ethane and characterized through several physicochemical techniques. Selected physicochemical characteristics of the prepared samples are included in Table 1.

Representative catalytic results of the differently synthesized NiO catalysts in the oxidative dehydrogenation of ethane are shown in Table 2. The reaction temperature used in this study has been fixed at 300 and 340 °C in order to have a better comparison of the catalytic performance of the catalysts, minimizing the effect of the reaction temperature in the selectivity to ethylene vs ethane conversion plot. Moreover, by not exceeding 350 °C in the reaction temperature, the modification of the catalysts heat-treated at the lowest calcination temperature is minimized.

In all cases, the only reaction products detected have been ethylene and CO_2. No carbon monoxide, acetic acid nor another O-containing product have been identified. An accurate carbon balance in the 98–102% range has been obtained in all the experiments.

Overall, the most active catalysts were those calcined at 350 °C with a catalytic activity ca. 3–4 times higher than that of the catalysts calcined at 500 °C. Moreover, a clear positive effect of the addition of oxalic acid has been observed regardless of the calcination temperature. Then, the addition of oxalic acid increases the reaction rate for ethane conversion by a factor of 2 (Fig. 1a). This increase is observed regardless of the amount of oxalic acid employed, so that the key factor of the catalytic activity is the presence or the absence of oxalic acid rather than its amount. As it can be seen in Table 2, the specific activity (activity normalized per surface area) is very similar for all catalysts regardless of the presence of oxalic acid or the calcination temperature used. Therefore, the surface area (i.e. the available active sites) seems to be the governing factor determining the catalytic activity.

Whenever there is not a drastic difference in reactivity, the key factor to be optimized in the catalytic performance for the oxidative dehydrogenation of ethane is the selectivity to ethylene. Then, Fig. 1b shows the values of the selectivity to ethylene at isoconversion conditions (10%). As it can be seen, the presence of oxalic acid in the synthesis gel leads to a remarkable increase in the selectivity to ethylene regardless of the calcination temperature. Then, the catalysts prepared in absence of oxalic acid present a selectivity of ca. 45–48% whereas that achieved on catalysts prepared in the presence of oxalic acid ranges between 63 and 75%. According to these results, the optimal catalysts were the ones prepared with an oxalic acid/nickel molar ratio of 1.0. Additionally, for a fixed oxalic acid/nickel molar ratio, the lower the calcination temperature the higher the selectivity to ethylene is.

Since the reactivity of the catalysts is different, we employed different contact times in order to obtain a comparative selectivity to ethylene vs. ethane conversion curve. Fig. 2 shows the variation of the selectivity to ethylene with the ethane conversion for selected catalysts. Noteworthy, in the range of conversions studied (until 20%) the fall in the selectivity to ethylene is not drastic. Therefore, it can be seen that the **Ni-1-350** catalyst presents the highest selectivity to ethylene, whereas **Ni-0-500** is the least selective.

Although there are many factors that define the catalytic performance of NiO based catalysts, the crystallite size has shown to have certain effect on both the catalytic activity and the selectivity [11,21,27–32,41]. Fig. 3 shows the XRD patterns of nickel oxide

Table 2
Oxidative dehydrogenation of ethane on undoped NiO catalysts.

Catalyst	C_2 conversion (%)	O_2 conversion (%)	Selectivity to ethylene (%)[a]	Catalytic Activity[a, b]	STY rate of ethylene formation [a, d]	Selectivity to ethylene (%) [e]	Specific activity [a, c]
Ni-0-350	7.0	42.3	49.5	513	239	49	7.3
Ni-0.8-350	13.2	59.4	66.6	967	606	68	8.8
Ni-1-350	12.6	49.7	72.8	922	633	73	13.2
Ni-1.5-350	11.8	53.2	66.6	865	542	69	11.4
Ni-3-350	13.7	61.3	66.9	1003	632	69	13.6
Ni-0-500	2.0	12.6	46.6	146	65	45	13.3
Ni-0.8-500	4.1	21.1	59.6	278	169	58	11.4
Ni-1-500	4.2	19.0	66.4	307	192	65	13.3
Ni-1.5-500	4.1	20.7	60.6	278	170	60	14.0
Ni-3-500	3.2	16.6	59.1	235	147	58	10.0

[a] C_2/O_2/He: 10/3.3/86.7 M ratio, reaction temperature = 340 °C, W/F = 4 g_{cat} h $(mol_{C2})^{-1}$; [b] in g_{C2H6} kg_{cat}^{-1} h^{-1}; [c] in 10^3 g_{C2H6} m^{-2} h^{-1}; [d] in g_{C2H4} h^{-1} kg_{cat}^{-1}; [e] Selectivity to ethylene at ethane conversion of 10%, 340 °C and variable contact times.

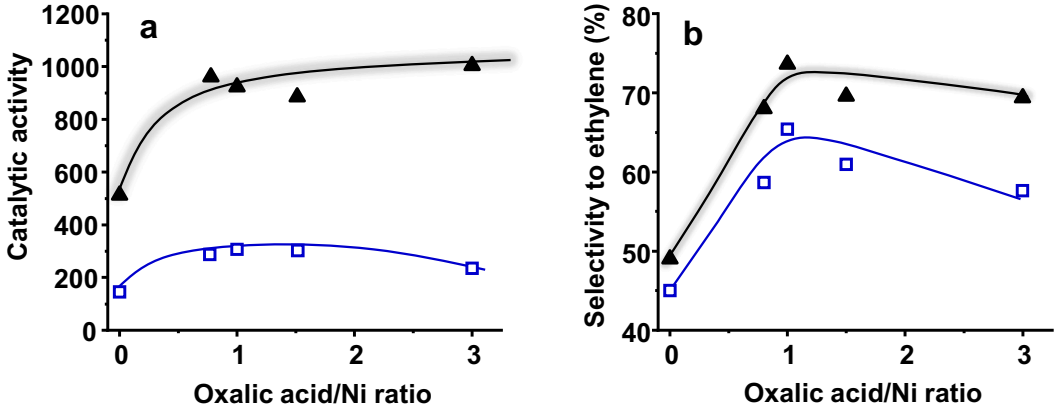

Fig. 1. Variation of: (a) the catalytic activity for ethane conversion, in $g_{C2H6}\ h^{-1}\ kg_{cat}^{-1}$; and (b) the selectivity to ethylene at 300 °C and isoconversion conditions with the oxalic acid/Ni ratio in the synthesis gel. Symbols: catalysts calcined at 350 °C (▲) or 500 °C (□) in air. Notes: Reaction conditions as in Table 2.

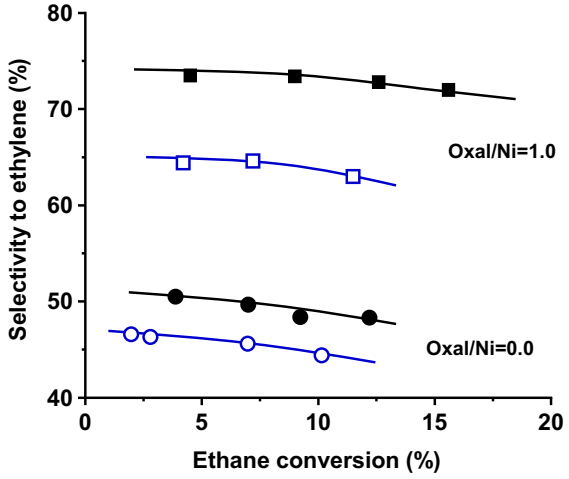

Fig. 2. Variation of the selectivity to ethylene with the ethane conversion during the ODHE at 300 and 340 °C over nickel oxide catalysts calcined at 350 °C (●, ■) and 500 °C (○, □). Catalysts: **Ni-0-350** (●); **Ni-0-500** (○); **Ni-1-350** (■); **Ni-1-500** (□). Reaction conditions in text.

catalysts calcined at 350 (Fig. 3a) or 500 °C (Fig. 3b). In all cases, the main peaks appear at 2θ: ~37.2, 43.2, 62.8, 75.3 and 79.3° which correspond to the (111), (200), (220), (311) and (222) planes of cubic NiO crystalline phase (JCPDS: 78–0643), respectively. The presence of partly (Ni_2O_3) or totally reduced (Ni^0) phases have not been detected. As it can be observed, all the samples present five intense peaks, regardless of the addition of oxalic acid and the calcination temperature, which have been considered to apply the Scherrer' Eq. [43].

However, interesting differences in terms of crystallinity are observed (Fig. S1, supporting information). Samples heat treated at 500 °C present narrow Bragg peaks which means that relatively large crystallites have been formed. Then, according to the Scherrer equation, a mean NiO crystallite size that varies from ca. 22 nm in the catalyst prepared without oxalic acid in the synthesis gel to ca. 17 nm in the catalysts prepared with oxalic acid in the synthesis gel has been determined (Table 1 and Fig. S1). As expected, the calcination at 350 °C leads to a widening of the Bragg peaks, which is related to material with lower crystallinity with tinier NiO crystallites. Then, average NiO crystallite size of ca. 12 nm in the catalyst prepared without oxalic acid decreased to 7–8 nm for those catalysts with moderated use of oxalic acid (oxalic acid/Ni ratio of 0.8 to 1.5). Finally, the use of higher oxalic acid loadings resulted in a further decrease of the average size since **Ni-3-350** presents an average size for NiO crystallites of ca. 5 nm. The determined crystallite sizes of the catalysts follow the trend expected considering their

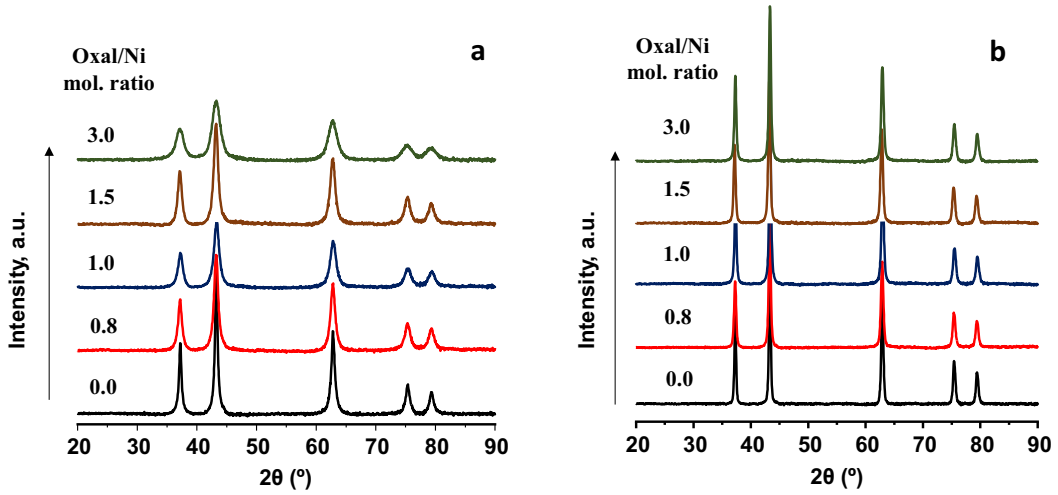

Fig. 3. XRD patterns of nickel oxide catalysts calcined at 350 °C (a) or 500 °C (b) with the oxalic acid/Ni molar ratio in the synthesis gel of: 0.0 (black), 0.8 (red), 1.0 (blue), 1.5 (brown) and 3.0 (green). (For interpretation of the references to colour in this figure legend, the reader is referred to the web version of this article.)

surface areas.

We must inform that the as-synthesized samples (before calcination) have been also characterized by XRD and Thermogravimetric analysis (Figs. S2 and S3, respectively, in the Supporting Information), in order to understand better the changes achieved in calcined samples, depending on the amount of oxalic acid in the synthesis gel. Thus, the XRD pattern of the as-synthesized samples indicates de presence of Nickel(II) nitrate hexahydrate ($Ni(NO_3)_{2\cdot 6\ H_2O}$, in the sample prepared without oxalic acid in the synthesis gel), whereas Nickel(II) oxalate dihydrate ($NiC_2O_{4\cdot 2\ H_2O}$) is mainly observed in samples prepared with oxalic acid in the synthesis gel (Fig. S2; Supporting information). This is also confirmed by Thermogravimetric analysis (Fig. S3; Supporting Information), in which the decomposition of Ni-nitrate (broad peak, not very intense) and Ni-oxalate (narrow peak, very intense) occurs at ca. 350 °C in TG.

The samples have been characterized by Visible Raman (using an excitation wavelength of 514 nm, Fig. S4) and UV Raman (using an excitation wavelength of 325 nm, Fig. 4), in order to differentiate the crystallinity and crystal sizes of catalysts.

Raman spectra of catalysts, using a 514 nm laser (Fig. S4), present main bands at 462 and 497 cm^{-1}, in addition to small broad bands at 710, 930 and 1081 cm^{-1}. Bands at 462 and 497 cm^{-1} have been assigned to the Ni—O stretching mode related to a rhombohedral deformation of the structure or to non-stoichiometric Ni—O [19,20,44]. The other bands have been related to overtones of the first ones or their combinations [20]. A small band at 1060 cm^{-1} is also observed in some cases, which can be related to the $\nu 1$ vibration mode of carbonate groups [20,45,46]. These results agree with previous ones on samples calcined at temperatures higher than 400 °C [19,20,44–46].

In addition to these, it can be also seen a shoulder at 410 cm^{-1} (especially in samples prepared with an oxalate/Ni ratio of 3.0), which could be related to the non-stoichiometry of catalysts and/or a higher nickel vacancy concentration [19,20]. On the other hand, the appearance of 2-magnon band (at ca. 1402 cm^{-1}) in samples calcined at 500 °C (Fig. 4a), which is absent in samples calcined at 350 °C, can be attributed to the transition from ferromagnetic to antiferromagnetic characteristics, in NiO materials calcined at temperatures higher than 400 °C [47,48].

Fig. 4 shows the UV Raman spectra of nickel oxide catalysts calcined at 350 or 500 °C, which can help to follow the spin-phonon interaction in these catalysts [48–50]. In general, it can be distinguished the presence of two main bands at ca. 571 and 1128 cm^{-1} (1145 cm^{-1} in samples calcined at 500 °C), which can be related to the one-phonon (1P) longitudinal optical (*LO*) mode and two-phonon (2P) longitudinal optical (*2LO*) mode, respectively, in NiO crystals [48,49]. In addition, two small bands are also observed at ca. 724 and 901 cm^{-1} related to two-phonon (2TO-transverse optical) and (TO) modes.

As it can be seen, the intensities of bands at ca. 571 and 1128 cm^{-1} change depending on the catalyst preparation procedure and/or calcination temperature. In this way, it has been proposed that the intensity of these most characteristic bands (1P *LO* band at ~571 cm^{-1} and 2P *2LO* band at ~1120 cm^{-1}) could be related to the specific structural and chemical features of the catalyst. Thus, an increase of the intensity of 2P *2LO* band (I_{1120}) higher than that of 1P *LO* band (I_{571}) is observed for catalysts calcined at 500 °C and for samples prepared without oxalic acid in the synthesis gel, suggesting that they present the higher NiO crystal size and/or the lower concentration of defects [51]. In an opposite trend, samples prepared in the presence of oxalic acid in the synthesis gel and calcined at 350 °C present the highest values of I_{571} and the lowest I_{1120}/I_{571} ratios. Accordingly, low I_{1120}/I_{571} ratios in the UV Raman spectra should correspond to samples presenting NiO particles with the lowest crystal size and/or the highest concentration of defects [50], being these aspects mainly related to the catalyst

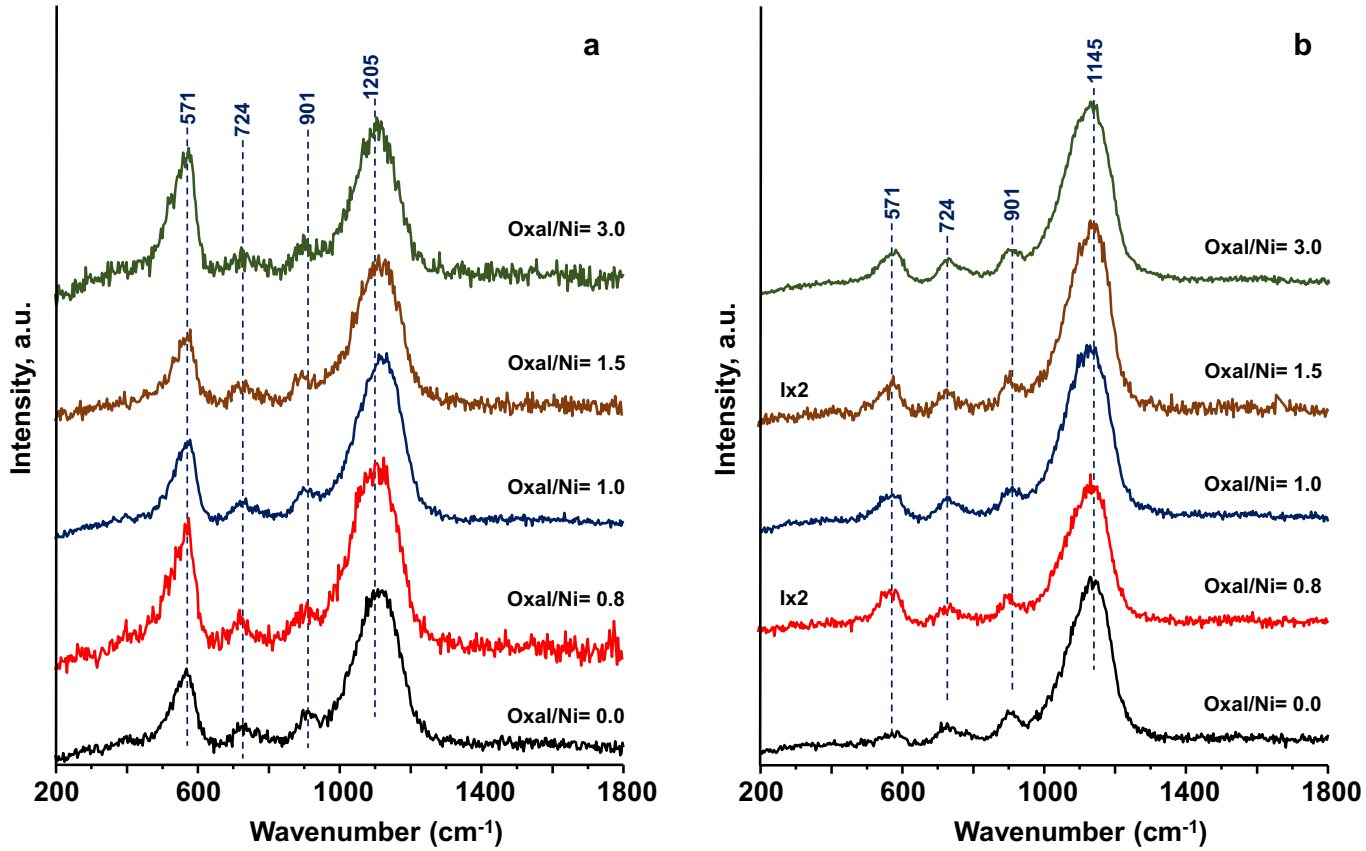

Fig. 4. UV Raman 325 nm spectra of NiO catalysts calcined at (a) 350 °C and (b) 500 °C with molar Oxalic acid/Ni ratio in the synthesis gel of: 0.0 (black), 0.8 (red), 1.0 (blue), 1.5 (brown) and 3.0 (green). (For interpretation of the references to colour in this figure legend, the reader is referred to the web version of this article.)

preparation (presence of oxalic acid in the synthesis gel) and/or lower calcination temperature. In the present work, a clear correlation between the relative intensity of the bands at 571 and 1120 cm^{-1} (I_{LO}/I_{2LO}) and the NiO crystallite size determined by XRD has been observed (Fig. S5). Therefore, an estimation of the concentration of over-stoichiometric oxygen in these catalysts is not straightforward to reach according to UV Raman spectroscopy.

The catalysts were also characterized by Diffuse Reflectance UV–vis spectroscopy (DRS). The DRS spectra of catalysts calcined at 350 or 500 °C are shown in Fig. 5. No distinguishable differences were observed in the UV area of the spectra, but some features can be observed in the visible area.

Several absorption bands have been observed (at 380, 416, 450, 650 and 722 nm) which are typical of bulk NiO [10,35,52,53] with Ni^{2+} in its octahedral coordination. In fact, it is well known that bulk NiO shows bands at 715, 420 and 377 nm, which can be related to the presence of octahedrally coordinated Ni^{2+} species in the cubic (rock-salt) NiO lattice [10,51,52]. In addition, a band at ca. 510 nm could be also related to charge transfer in NiO crystals [53,54]. On the other hand, and although there is not a clear trend in these spectra, it can be observed a higher intensity of the absorption in the 400–600 nm range for the catalysts calcined at 350 °C (Fig. 5A) than those at 500 °C (Fig. 5B). This is especially notorious in the sample prepared in the absence of oxalic acid in the synthesis gel (i.e. **Ni-0-350**). A high background absorbance for this area has been linked with a high concentration of non-stoichiometric oxygen. Therefore, it seems that those samples calcined at 350 °C, and especially **Ni-0-350**, present the highest amount of non-stoichiometric oxygen.

A detailed study of these catalysts was also undertaken through TEM and High Resolution TEM (Fig. 6). Catalysts calcined at 350 °C show drastic differences when adding oxalic acid in the synthesis. The basic **Ni-0-350** catalyst presents large agglomerations of several micrometres consisting of highly porous poorly defined particles of variable size, ranging from large (50 nm) to small (5 nm) particles. The **Ni-1-350** sample presents well defined particles with sizes between 5 and 50 nm. Interestingly, small cavities in the range of 1–2 nm are located within these particles. In the inset of Fig. 6b, it is observed by HR-TEM some ca. 10–15 nm particles with tiny cavities. Finally, the sample prepared with the highest concentration of oxalic acid (sample **Ni-3-350)** is formed by tiny particles with a rather uniform size (ca. 4 nm) and aspect. In the inset of Fig. 6c, small 3 to 6 nm particles are clearly observed in close contact with each other.

Fig. 6 shows also selected TEM/HRTEM images of NiO catalysts calcined at 500 °C. Overall, the effect of the oxalic acid is similar to that observed for catalysts calcined at 350 °C but at 500 °C the porosity and the presence of cavities is much lower. This fits with the decreased surface area observed in the latter. **Ni-0-500** catalyst has large agglomerations of rather big particles without apparent porosity and a few small nanoparticles of 10 nm and less (Fig. 6d). **Ni-1-500** presents well defined particles most of them between 10 and 30 nm of diameter without apparent internal cavities (Fig. 6e). Finally, **Ni-3-500** shows well defined particles and a similar morphology but with slightly smaller particles than that sample with lower oxalic acid content (Fig. 6f).

SAED patterns (Fig. S6) demonstrate that all NiO catalysts are formed by crystalline Ni-containing nanoparticles, which can be indexed unambiguously to cubic NiO. No metallic Ni nor Ni_2O_3 were identified. A further analysis indicates that the lattice parameter ranges from 0.419 nm to 0.416 nm (see Table 1) and a clear effect of the preparation procedure on this value has not been observed. However, by taking separately both calcination temperatures, a decrease of the lattice

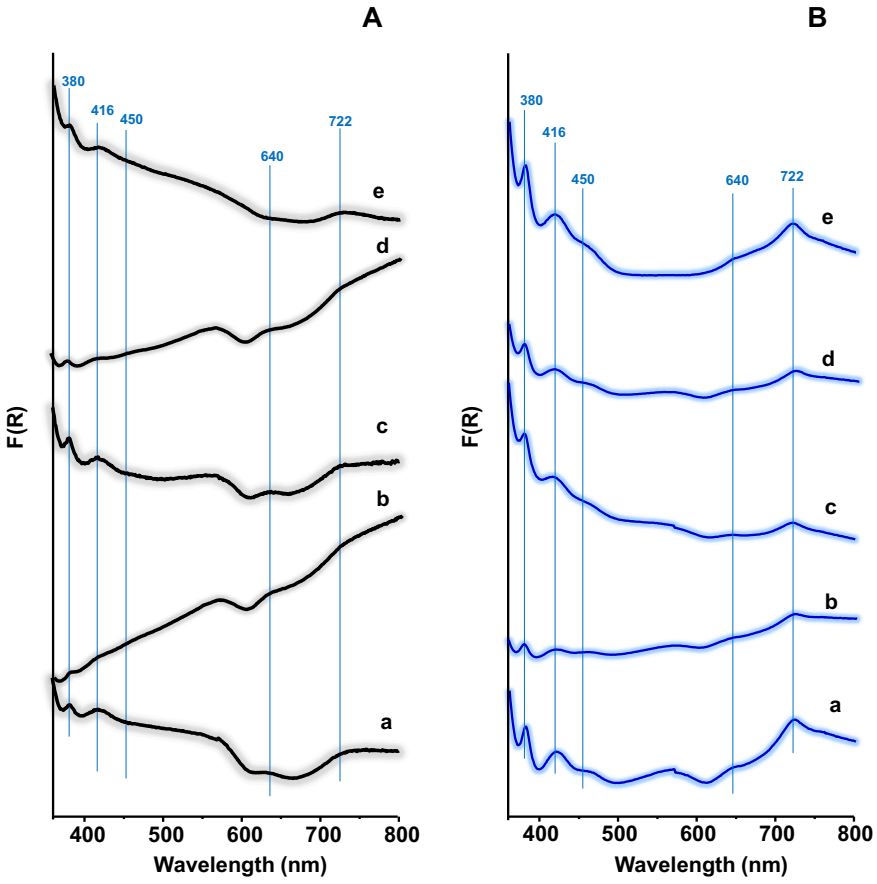

Fig. 5. DR-UV–Vis spectra of NiO catalysts, calcined at 350 °C (A) or 500 °C (B), prepared with an oxalic acid/Ni ratio in the synthesis gel of: (a) 0.0; (b) 0.8; (c) 1.0; (d) 1.5; and (e) 3.0.

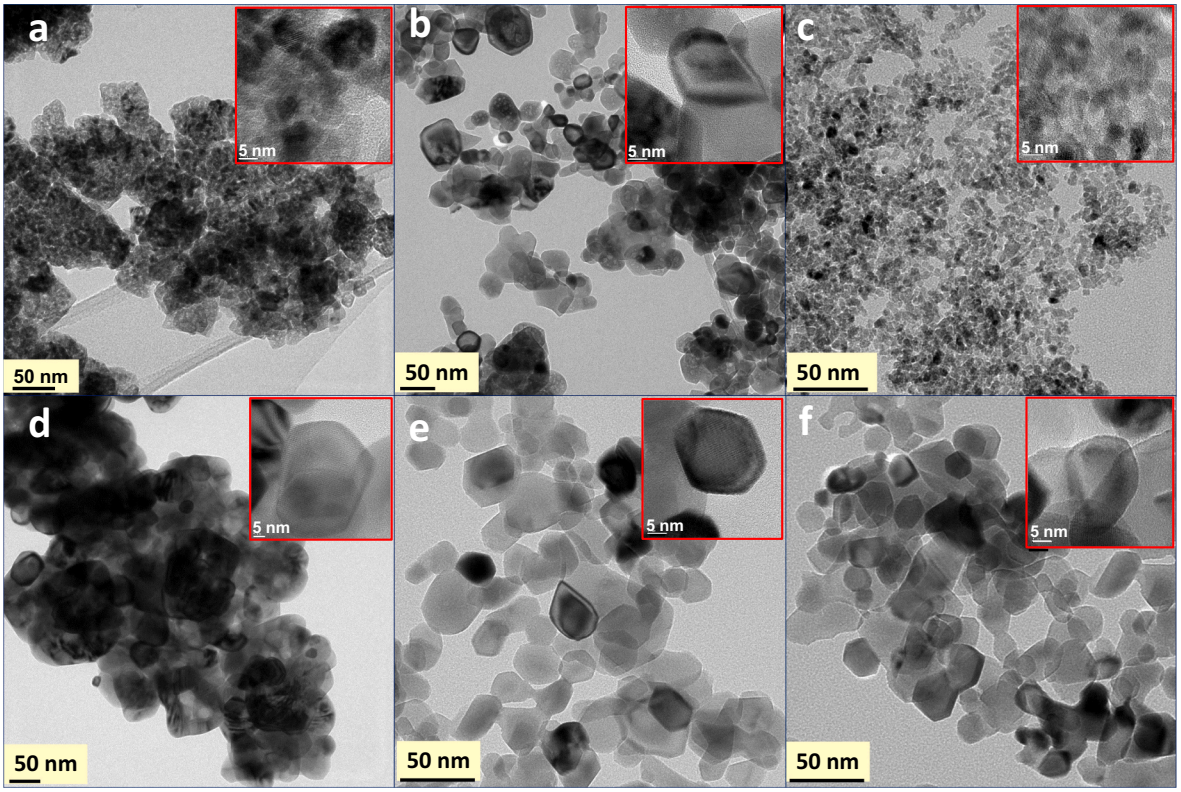

Fig. 6. TEM and HR-TEM micrographs of NiO catalysts: a) **Ni-0-350**; b) **Ni-1-350**; c) **Ni-3-350**; d) **Ni-0-500**; e) **Ni-1-500**; f) **Ni-3-500**.

parameter has been observed in the samples treated with oxalic acid. In this way, the decreased particle size could partially explain the decrease lattice parameter observed.

The reducibility of the NiO catalysts has been also studied by temperature programmed reduction (Fig. 7) as it can influence the catalytic performance of this type of catalysts [11,19–21,27–33,54–57]. Thus, the oxidative dehydrogenation of ethane takes place by a redox mechanism [57], being the reduction part considered as the limiting step at moderate and high temperatures. Then, the catalytic activity in this reaction could be related to the reducibility of the sample. Moreover, it has been proposed for many NiO based catalysts [11,19–21,27–33,54–57] that the most selective sites are the ones that present the lowest reducibility.

Overall, the reduction profile of these catalysts is rather similar with a broad reduction peak centred between 254 and 351 °C. This broad peak, which can contain a shoulder, has been related to the reduction of bulk NiO (lattice oxygen) [55– 57]. Interestingly, the onset temperature for this band takes place at similar temperatures regardless of the catalyst, but the maximum shifts towards lower temperatures when the amount of oxalic acid used increases. It is noteworthy the presence of a low intensity reduction band at ca. 200 °C.

This band at 200 °C has been reported to be related to the reduction of over-stoichiometric oxygen, i.e. Ni^{3+} species or even Ni_2O_3 [29,56]. An enlargement of the area around 200 °C (see Fig. 7) shows that the low temperature band is especially intense in the samples calcined at 350 °C and, above all, in the reference catalyst (sample **Ni-0-350**). However, the use of oxalic acid in the synthesis gel leads to a decrease in its height. This reduction peak, with low intensity, can be also observed in the reference sample calcined at 500 °C (sample **Ni-0-500**) but not in the other catalysts.

The hydrogen consumption observed during the TPR experiments slightly exceeds the hydrogen necessary to completely reduce $Ni^{2+}O$ into metallic Ni (102–105% of the theoretical $NiO + H_2 \rightarrow Ni + H_2O$ reaction). However, a defined trend regarding calcination temperature or presence of oxalic acid has not been detected. Nevertheless, this higher hydrogen consumption could indicate that these catalysts present an excess of oxygen over the stoichiometric NiO.

The surface of the nickel oxide catalysts has been characterized by XPS of samples calcined at 350 or 500 °C. Fig. 8 shows the Ni $2p_{3/2}$ core level spectra for the catalysts calcined at 350 °C (Fig. 8a) and 500 °C (Fig. 8b), respectively. In all cases, the spectra show a wide band centered at ca. 854.5 eV. This band presents two maxima. The first one (usually referred as Main Peak) at binding energy ca. 853 eV is attributed to structural Ni^{2+} species. The second maximum corresponds to a satellite (usually referred as Sat I) that appears at 855 eV and it is related to the presence of multiple defects in the structure (i.e. Ni^{2+} vacancies, Ni^{3+} and/or Ni^{2+}-OH species) but also to nickel atoms not coming from lattice oxygen-nickel bound but from octahedral NiO_6 neighbour cluster units [57,58]. A second wide satellite (Sat II) with its maximum at 860.2 eV is associated to ligand-metal charge transfer [28,36,57,58].

The relative intensity of the Sat I compared to the Main peak (Sat I/Main peak ratio) has been determined by the deconvolution of the wide band into two bands (centered at 853 and 855 eV). This ratio has been roughly related to the presence of nickel defects [27]. As it can be seen, and in accordance with the XRD results, lower calcination temperatures lead to worst crystallization of the NiO regardless of the oxalic acid amount, and therefore, higher presence of nickel defects, as it can be stated for the higher Sat I / Main Peak relationship of their relative intensity values (see Table 3). However, the Sat I / Main Peak relationship for the catalysts treated at 500 °C leads to fairly lower values, suggesting that a severe thermal treatment favors better crystallization of the catalysts. Regrettably, due to the uncertainty of the assignment of Ni bands accurate conclusions cannot be drawn.

On the other hand, Fig. 8 shows also the O *1s* core level XPS spectra of the NiO catalysts calcined at 350 °C (Fig. 8c) and 500 °C (Fig. 8d). In our case, it can be differentiated three types of signals [41,59,60]: the first one (O_I) at binding energy of ca. 528.6 eV is the majority and it is related to structural nucleophilic lattice oxygen species; the second one (O_{II}) appears at 530.5 eV, and it is attributed to OH^- species; and finally,

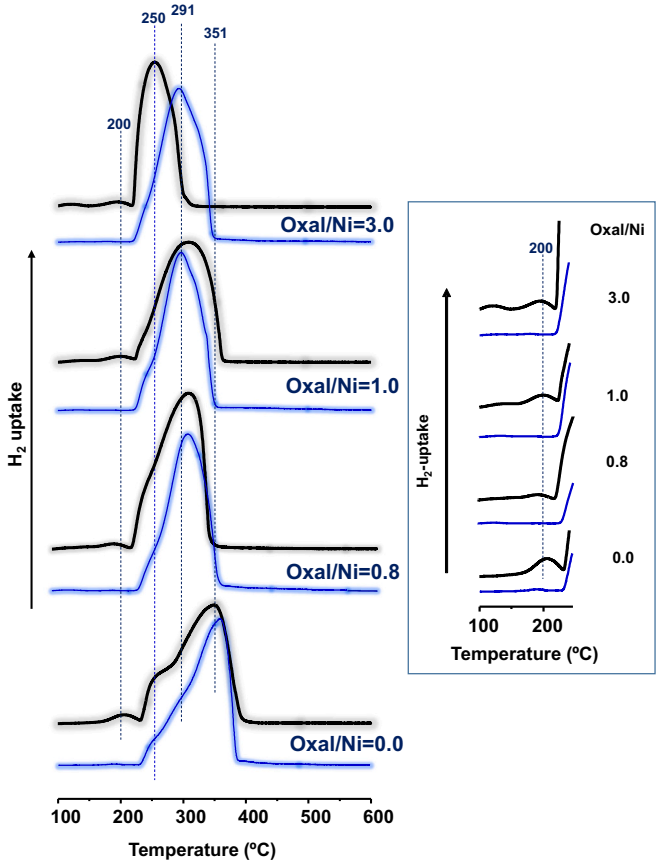

Fig. 7. Temperature programmed reduction profiles for NiO catalysts, calcined at 350 (black) or 500 °C (blue), prepared with oxalic/Ni ratios in the synthesis gel of: 0.0; 0.8; 1.0; or 3.0. (For interpretation of the references to colour in this figure legend, the reader is referred to the web version of this article.)

the third signal (O_{III}) at 532.5 eV is ascribed to electrophilic (O_2^- and/or O^{-}) species on the surface of the catalysts. Table 3 shows the relative proportion of these oxygen species.

According to these results, those catalysts calcined at 350 °C present a similar concentration of nucleophilic species (51–60%), those catalysts with an oxalic acid/Ni ratio of 1 presenting the highest concentration. In addition, it is clear that the signal corresponding to OH^-/defects (O_{II}) is more intense in the catalysts calcined at 350 °C to the detriment of the electrophilic oxygen (O_{III}) signal (Table 3), which are shown to be responsible for the deep oxidation of the paraffin [62].

These results are in good agreement with all the characterization reported above and suggests that a lower presence of electrophilic species enhance the selectivity to the partial oxidation product.

In order to get more information about the number of vacancies we have decided to evaluate the semiconductor behaviour of the catalysts through Mott-Schottky plots (see conditions in Experimental section). Mott-Schottky plots represent the reciprocal of the square capacitance vs the applied potential. In particular, the Mott-Schottky equation for a p-type semiconductor (such as NiO [63]) is the following:

$$\frac{1}{C^2} = \frac{1}{C_H} - \frac{2}{\varepsilon_r \cdot \varepsilon_0 \cdot e \cdot N_A}\left(E - E_{FB} - \frac{kT}{e}\right) \quad (1)$$

where C is the value of total interfacial capacitance calculated from EIS, C_H is the capacitance of the Helmholtz layer, ε_r is the dielectric constant of the semiconductor used as a catalyst (~12 for nickel oxide) [64], ε_0 is vacuum permittivity ($8.85 \cdot 10^{-14}$ F cm^{-1}) and e is the electron charge ($1.60 \cdot 10^{-19}$C), N_A is the density of acceptors in the semiconductor, E is the applied potential, E_{EF} is the flat-band potential, k is the Boltzmann constant ($1.38 \cdot 10^{-23}$ J/K) and T is the absolute temperature. From the slope of the linear region of the Mott-Schottky plots, N_A values for the different catalysts can be calculated.

Mott-Schottky plots for the catalysts with and without oxalic acid in the synthesis gel are presented in Fig. 9. It is observed that, for all the catalysts, a linear region with a negative slope is displayed in the Mott-Schottky plots, which is characteristic of p-type semiconductors with an excess of cationic vacancies [64–67], the predominant defect type in NiO [41].

Fig. 9 also shows the value of the acceptor densities calculated for catalysts calcined at 350 or 500 °C, synthesized with or without oxalic acid in the synthesis gel. Independently of the oxalic acid content in the synthesis gel, N_A values are in general higher for catalysts calcined at 350 °C but the presence of oxalic acid clearly diminished the number of N_A with respect to the base NiO catalyst (i.e. **Ni-0-350**), regardless of the calcination temperature (Table 1). This confirms that catalysts prepared with oxalic acid in the synthesis gel present less cationic vacancies, which are related with the excess of non-stoichiometric oxygen, i.e. mainly electrophilic oxygens [11,41,57].

These electrochemical results are in good agreement with the DRS and H_2-TPR measurements, where the highest amount of non-stoichiometric oxygen species correspond to the catalysts synthesized without oxalic acid in the gel solution and calcined at 350 °C. Additionally, acceptor densities are consistent with XRD and XPS results, since catalysts obtained at low calcination temperatures presented the highest concentration of nickel defects.

4. Discussion

In the present article we have demonstrated that by controlling the calcination temperature and adding oxalic acid in the synthesis gel, a rather unselective material as unsupported and unpromoted NiO can turn into a selective catalyst for the oxidative dehydrogenation of ethane. A 73% selectivity to ethylene at 10% of ethane conversion as well as a highly stable behaviour has been reached with the optimal catalyst.

Several factors have been shown to influence the catalytic performance (and more importantly, the selectivity to ethylene) of NiO-based catalysts. Tiny NiO crystallites seem to be desirable to obtain high selectivity to ethylene in promoted NiO catalysts [19–21,27–32] although in supported catalysts this trend is not clear [33–36]. In those cases, the nature of the support and the NiO-support interaction play an important role.

Fig. 10 shows the influence of the average NiO crystallite size over the selectivity to ethylene. It can be observed that, among those samples calcined at a given temperature, the catalysts with the lowest size are the most selective ones. However, it is not a general trend.

For example, the catalyst prepared in the absence of oxalic acid calcined at 350 °C presents a selectivity lower than 50% with a mean crystallite size of ca. 12 nm and those prepared with oxalic acid at 500 °C can reach 66% selectivity with a size of ca. 18 nm. Therefore, other factors are involved in the enhanced performance of the catalysts synthesized in the presence of oxalic acid.

Recently, Zhao et al. [41] studied pure NiO catalysts heat-treated at different temperatures between 400 and 1000 °C and observed a direct correlation between the amount of non-stoichiometric oxygen and the selectivity to the olefin. This observation contrasts with that reported previously in different articles. Relationships between nucleophilic oxygen and the formation of partial oxidation and dehydrogenation products, as well as electrophilic oxygen and formation of total oxidation products, have been often proposed [11,21,61,68,69]. In the case of electrophilic oxidation, it proceeds through the activation of the molecular oxygen fed favouring the formation of cracking products and carbon oxides (total oxidation is highly favoured). Conversely, nucleophilic oxygen tends to attack C—H bonds in a previously activated organic molecule, maintaining the same size of the hydrocarbon. In this

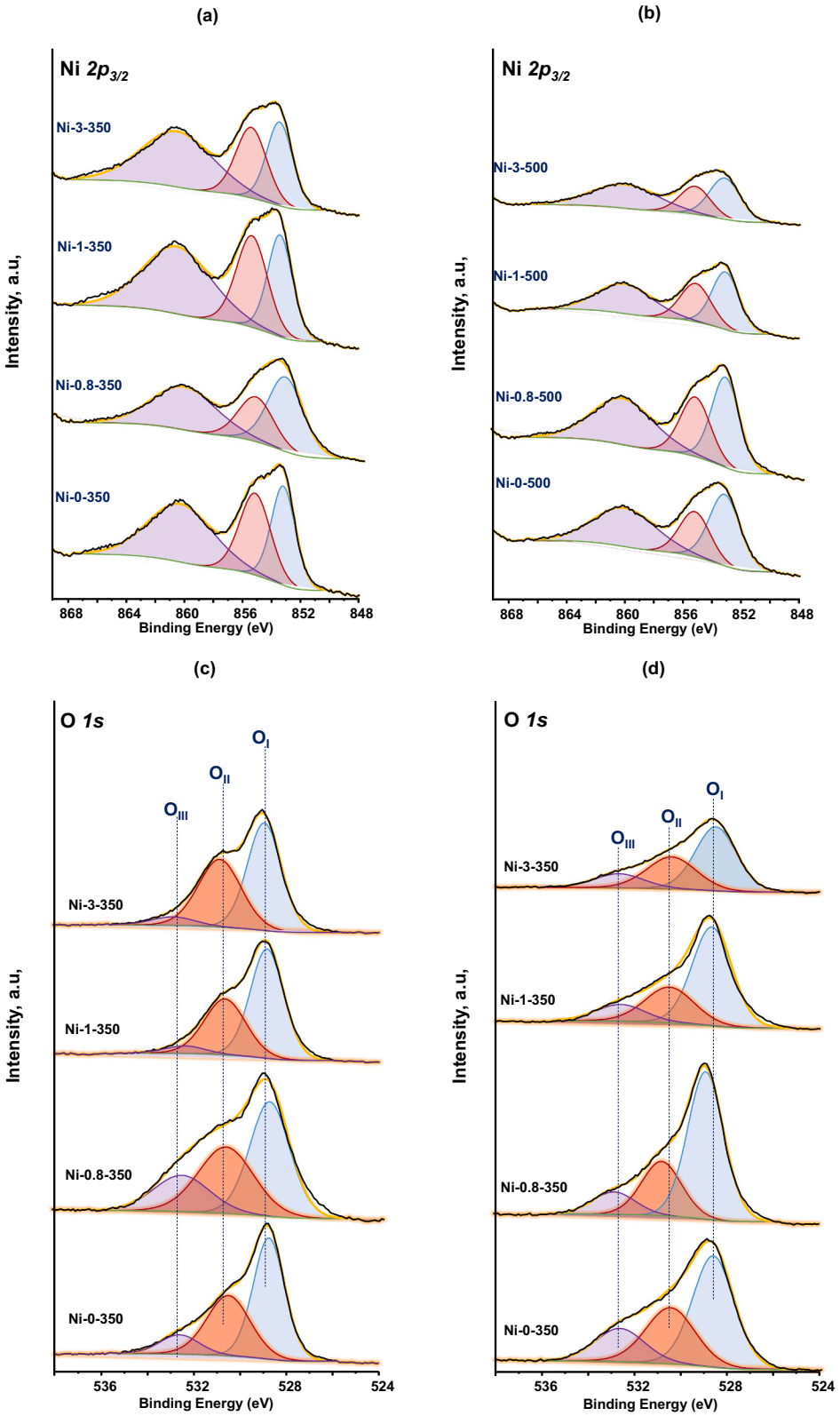

Fig. 8. XPS results of selected catalysts calcined at 350 (a and c) or 500 °C (b and d). Ni $2p_{3/2}$ core level spectra (a and b); O *1 s* core level spectra (c and d).

sense, non-stoichiometric oxygen is more electrophilic than lattice oxygen, so that one could think that catalysts with high concentration of oxygen in excess tends preferentially to transform ethane into carbon oxides. In fact, several authors have found in promoted NiO catalysts that the decrease in the amount of non-stoichiometric oxygen leads to an enhanced selectivity to ethylene [19–21,27–31,70]. Similarly, it was demonstrated an inverse relationship between the selectivity to the olefin in promoted NiO catalysts with the p-conductivity [19,39,70]. Accordingly, NiO doped with high valence promoters (+4 and above) have been reported to be the most selective catalysts for the olefin

Table 3
XPS results of nickel oxide catalysts.

Catalyst	Ni $2p_{3/2}$	O *1 s*			Ni/O surface
	Sat-I/M.P.	O_I (%)	O_{II} (%)	O_{III} (%)	atomic ratio, %
Ni-0-350	1.06	53	36	11	0.62
Ni-0.8-350	0.60	44	36	20	0.49
Ni-1-350	1.13	58	37	5	0.81
Ni-3-350	1.00	53	42	5	0.67
Ni-0-500	0.64	51	31	18	0.46
Ni-0.8-500	0.72	63	26	11	0.35
Ni-1-500	0.75	60	27	13	0.47
Ni-3-500	0.68	54	32	14	0.53

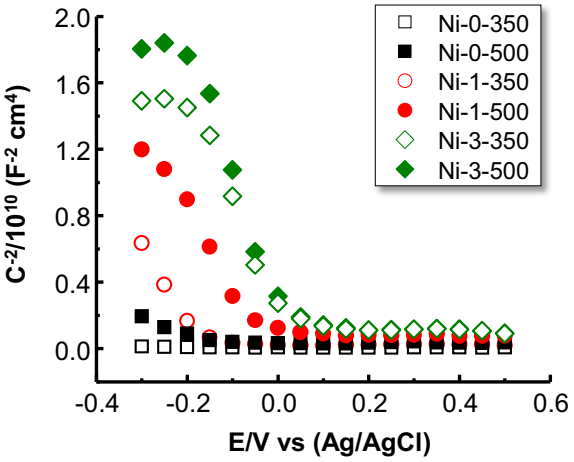

Fig. 9. Mott-Schottky plots for NiO catalysts (prepared with an oxalic acid/Ni ratio in the synthesis gel of 0.0, 1.0 or 3.0) and calcined at 350 or 500 °C. Characteristics of catalysts in Table 1.

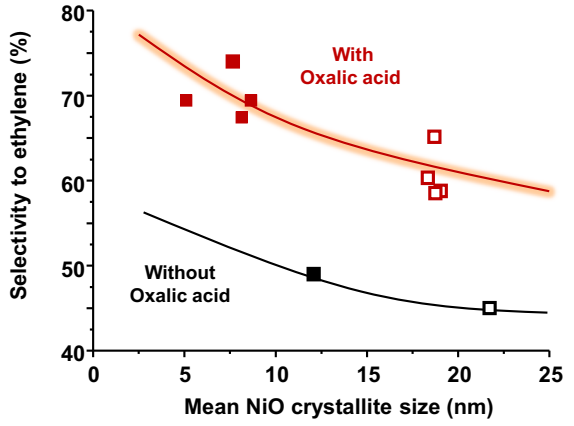

Fig. 10. Relationship between the mean NiO crystallite size and the selectivity to ethylene. Notes: size estimated by XRD (Table 1) and the values of selectivity to ethylene were taken at 300 °C and 10% ethane conversion (Table 2). Symbols: Catalyst prepared in the presence (red) or absence (black) of oxalic acid; and calcined at 350 (full symbols) or 500 °C (empty symbols). (For interpretation of the references to colour in this figure legend, the reader is referred to the web version of this article.)

formation, but they also provoke a decrease of the mean oxidation state of Ni, consequently decreasing the amount of non-stoichiometric oxygen [11,19–21,27–32]. In the same way, it has been shown for supported NiO catalysts that the selectivity to ethylene increases concomitantly when the number of Ni neighbours in the first (Ni—O) and the second coordination shell (Ni—Ni) decreases [33]. The elimination of surface electrophilic species (which is somewhat related to the density of over stoichiometric oxygen) has been also linked to a higher ethylene formation in supported or promoted Nb- and Ti- doped NiO catalysts [41].

Most of these studies have been focused in promoted or supported NiO since undoped bulk NiO usually presents a poor performance with a massive formation of carbon dioxide. Maybe, in those cases, the role of the promoter and/or the support has been underestimated. In the present article several pure NiO catalysts have been tested, being the catalysts calcined at 350 °C the ones that present the highest concentration of non-stoichiometric oxygen. As expected, the amount of non-stoichiometric oxygen decreased when the calcination temperature increases [71]. However, the most selective catalysts are those prepared with oxalic acid and, although the calcination temperature plays a role, it is upset by the effect of the use of oxalic acid. The presence of oxalic acid in the synthesis gel also leads to a decrease in the concentration of overstoichiometric oxygen species. This is due to the reductant behaviour of the oxalic acid, which favors the Ni^{3+} to Ni^{2+} transition. However, this elimination of non-stoichiometric oxygen when using oxalic acid takes place to a lesser extent than by increasing the calcination temperature. Therefore, no relationship has been observed between the amount of non-stoichiometric oxygen and the selectivity to ethylene.

Fig. 11 shows the evolution of the ethane conversion and the selectivity to ethylene with the time on line for **Ni-1-350** and **Ni-1-500** catalysts together with the DR-UV–Vis. spectra of these catalysts before and after use. It can be seen that, after 9 h of use the catalytic performance kept invariable, maintaining both the same conversion and selectivity.

Interestingly, the UV–Vis. spectra of the used catalysts changed with respect to the fresh catalysts since the absorbance in the 450–600 nm range, which is qualitatively related to non-stoichiometric oxygen, is remarkably lower. Then, after a moderate use in an atmosphere with ethane and oxygen (9 h with an ethane/O_2 ratio = 3 M), the catalysts seem to lose part of the over-stoichiometric oxygen. This is in agreement with the decrease in the oxygen excess observed in Nb-doped NiO catalysts after their use in the oxidative dehydrogenation of ethane [29,72]. In our case, the loss of oxygen in excess has not meant a drop of either catalytic activity or selectivity to ethylene.

The apparent contradiction observed in different works about the need for the presence or absence of non-stoichiometric oxygen can be due to the fact that electrophilic oxygen species have been reported to be the ones that activate the ethane molecule [73]. Thus, these electrophilic species would be necessary for the activation of the ethane, but they should be isolated (and, therefore, be present in low concentration) to avoid the transformation of ethane into carbon dioxide. Accordingly, surface area should also play a role as higher surface areas would allow a higher dispersion of electrophilic species. Perhaps, due to the need for electrophilic species to activate the ethane molecule, NiO based catalysts have not been described in the literature to present consistent selectivity to ethylene above 95%. Hence, a general correlation between the concentration of electrophilic oxygen and the selectivity to ethylene is not direct and will depend on other factors such as the surface area, the presence of promoters or supports or even to the different morphologies and exposed planes.

As mentioned above, it has been proposed in several articles that in supported or promoted NiO based catalysts [11,19–21,27–33,54–57] the most selective sites are those with the lowest reducibility. However, in the present work, the study of unpromoted bulk NiO does not show a clear correlation although the least selective catalysts (the ones without oxalic acid in the synthesis gel) are those that show the highest reduction maxima temperature, according to our H_2-TPR assays.

On the other hand, considering that the reduction band at 200 °C of the TPR experiments is related to non-stoichiometric oxygen (Ni^{3+}-like species), the extent of isolation of electrophilic species could be roughly estimated by dividing that area by the specific surface area of each catalyst. Then, for a given calcination temperature the most selective catalysts are those in which non-stoichiometric oxygen concentration (normalized per surface area) is lower, i.e., non-stoichiometric oxygens

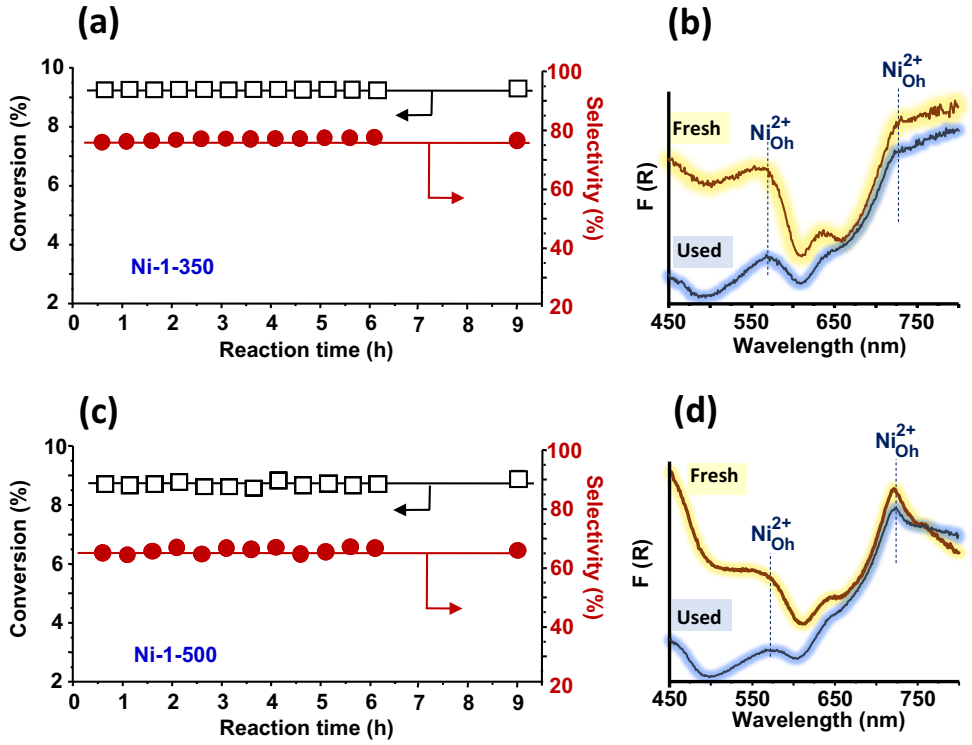

Fig. 11. Ethane ODH stability study over **Ni-1-350** (a) and **Ni-1-500** (c) catalysts with the corresponding DR-UV–Vis (b and d, respectively) spectra of fresh and used catalysts. **Notes:** Reaction temperature = 300 °C; W/F = 15 g_{cat} h mol_{C2}^{-1} (**Ni-1-350**) or 75 g_{cat} h mol_{C2}^{-1} (**Ni-1-500**). Remaining reaction conditions in text.

are more isolated (Fig. 12a). In any case, samples calcined at 350 °C present higher selectivity than samples calcined at 500 °C.

As mentioned in the Results section, cationic vacancies have been estimated through an electrochemical assay determining the N_A value (acceptor density). This N_A value turned out to be higher for catalysts calcined at 350 °C; although the presence of oxalic acid in the synthesis gel also leads to a decrease of the N_A value. Thus, Fig. 12b shows the relationship between the selectivity to ethylene with the acceptor density values for the three set of catalysts, i.e. catalysts prepared with an oxalic acid/Ni molar ratio of 0, 1.0 or 3.0, and calcined at 350 or 500 °C. It can be clearly observed that the highest selectivity to ethylene is related to lower acceptor densities (in Fig. 12b). In particular, the catalysts synthesized with oxalic acid show lower N_A values, that is, the lowest concentration of cationic vacancies. Hence, catalysts prepared with oxalic acid have less concentration of non-stochiometric oxygen which, in turn, could overoxidize ethane to non-desired carbon compounds, such as CO_2.

The main achievement of the present article is that the simultaneous use of low calcination temperatures and a certain amount of oxalic acid leads to the formation of highly selective undoped NiO catalysts which additionally are very stable.

The characterization of as-synthesized samples (before calcination) suggests important changes depending on the absence or presence of oxalic acid in the synthesis gel. Thus, Ni-nitrate was observed in the

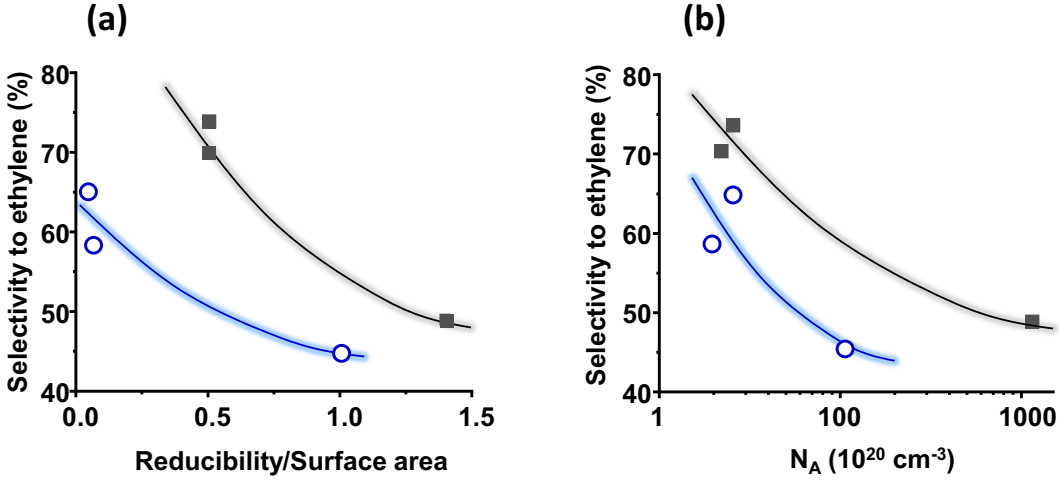

Fig. 12. Variation of the selectivity to ethylene with the reducibility/surface area (a) or with the acceptor density (b). Reducibility/surface area, in a.u., was calculated from the area of the reduction peak at ca. 200 °C divided by the surface area. Acceptor density as in Table 1. Selectivity to ethylene at 10% conversion (Table 2). Symbols: (■) calcined at 350 °C, (o) calcined at 500 °C.

sample prepared without oxalic acid in the synthesis gel, whereas Ni-oxalate is observed in the precursors of catalysts prepared with oxalic acid in the synthesis (Fig. S2, in the Supporting information). These differences, which determine also a different behaviour during the thermal decomposition of precursors (Fig. S2, in the Supporting information) should have an important influence on the physicochemical characteristics, and then, on the catalytic properties of the calcined catalysts [74,75], especially in samples calcined at 350 °C.

In addition, these catalysts also present high catalytic reactivity, making it possible for them to operate at low reaction temperatures (ca. 300 °C) with a negligible loss of activity. This high stability contrasts with that reported in several articles in which a certain deactivation is observed in the ODH of ethane using NiO based catalysts. Deactivation has been related in former articles to formation of mixed inactive phases such as $NiWO_4$ [72] or $NiNb_2O_6$ [20], the reduction of NiO over-stoichiometric oxygen [20] and the decrease in the surface area [73]. In our catalysts, no mixed phases can be formed since the only chemical element present in these catalysts, apart from oxygen, is nickel. Interestingly, we have observed an apparent decrease in the amount of non-stoichiometric oxygen after using the optimal NiO catalyst, which, on the contrary, has had no effect on catalytic activity and ethylene selectivity.

5. Conclusions

A non-promoted and non-supported NiO catalyst active and with a reasonably high selectivity to ethylene in the oxidative dehydrogenation of ethane has been prepared. The joint use of low calcination temperature (350 °C) and the inclusion of an appropriate oxalic acid loading in the synthesis gel during the preparation procedure has led to notable selectivity to ethylene (ca. 73%). Interestingly, a stable catalytic performance with the time on line has been observed in the optimal catalysts. This high stability can be related to the low reaction temperature required to undertake the reaction. The use of oxalic acid in the synthesis gel has been shown to highly improve the catalytic performance as an increase in the selectivity to ethylene by ca. 25 points and the reactivity by a factor of 1.5–2.0 compared to the reference sample have been obtained. Moreover, the calcination temperature has been shown as a determining factor in a way that catalysts calcined at 350 °C are more active and more selective to ethylene than analogous catalysts calcined at 500 °C. The enhanced catalytic performance of catalysts prepared in the presence of oxalic acid has not been only related to the NiO crystallite size and, more interestingly, the amount of electrophilic oxygen does not seem to play alone a determining role in the selectivity to ethylene. However, although a precise correlation has not been obtained, the most selective catalysts present high extent of isolation of non-stoichiometric oxygen and low p-type semiconductor character.

CRediT authorship contribution statement

Yousra Abdelbaki: Investigation, Formal analysis. **Agustín de Arriba:** Investigation, Formal analysis. **Rachid Issaadi:** Methodology, Supervision. **Rita Sánchez-Tovar:** Methodology, Investigation, Formal analysis. **Benjamín Solsona:** Conceptualization, Supervision, Writing – review & editing. **José M. López Nieto:** Conceptualization, Project administration, Writing – review & editing.

Declaration of Competing Interest

The authors declare that they have no known competing financial interests or personal relationships that could have appeared to influence the work reported in this paper.

Acknowledgements

Authors would like to acknowledge the Ministerio de Ciencia, Innovación y Universidades in Spain through projects CRTl2018-099668-B-C21 and MAT2017-84118-C2-1-R. A.A. acknowledges Severo Ochoa Excellence Program for his fellowship (BES-2017-080329). Y.A. and R.I. thank the Ministry of Higher Education and Scientific Research of Algeria for the National Exceptional Program for the fellowships.

Appendix A. Supplementary data

Supplementary data to this article can be found online at https://doi.org/10.1016/j.fuproc.2022.107182.

References

[1] S. Najari, S. Saeidi, P. Concepcion, D.D. Dionysiou, S.K. Bhargava, A.F. Lee, K. Wilson, Oxidative dehydrogenation of ethane: catalytic and mechanistic aspects and future trend, Chem. Soc. Rev. 50 (2021) 4564–4605, https://doi.org/10.1039/d0cs01518k.
[2] Y. Gao, L. Neal, D. Ding, W. Wu, Ch. Baroi, A.M. Gaffney, F. Li, F., Recent advances in intensified ethylene production- a review, ACS Catal. 9 (2019) 8592–8621, https://doi.org/10.1021/acscatal.9b02922.
[3] O.O. James, S. Mandal, N. Alele, B. Chowdhury, S. Maity, Lower alkanes dehydrogenation: Strategies and reaction routes to corresponding alkenes, Fuel Process. Technol. 19 (149) (2016) 239–255, https://doi.org/10.1016/j.fuproc.2016.04.016.
[4] I. Amghizar, L.A. Vandewalle, K.M. Van Geem, G.B. Marin, New trends in olefin production, Engineering 3 (2017) 171–178, https://doi.org/10.1016/J.ENG.2017.02.006.
[5] L. Brody, L. Neal, V. Haribal, F. Li, Ethane to liquids via a chemical looping approach - Redox catalyst demonstration and process analysis, Chem. Eng. J. 417 (2021) 128886, https://doi.org/10.1016/j.cej.2021.128886.
[6] J.T. Grant, J.M. Venegas, W.P. McDermott, I. Hermans, Aerobic oxidations of light alkanes over solid metal oxide catalysts, Chem. Rev. 118 (2018) 2769–2815, https://doi.org/10.1021/acs.chemrev.7b00236.
[7] J.M. López Nieto, P. Botella, P. Concepción, A. Dejoz, M.I. Vazquez, Oxidative dehydrogenation of ethane on Te-containing MoVNbO catalysts, Catal. Today 91-92 (2004) 241–245, https://doi.org/10.1016/j.cattod.2004.03.040.
[8] P.J. Donaubauer, D.M. Melzer, K. Wanninger, G. Mestl, M. Sanchez-Sanchez, J. A. Lercher, O. Hinrichsen, Intrinsic kinetic model for oxidative dehydrogenation of ethane over MoVTeNb mixed metal oxides: A mechanistic approach, Chem. Eng. J. 383 (2020) 123195, https://doi.org/10.1016/j.cej.2019.123195.
[9] T. Konya, T. Katou, T. Murayama, S. Ishikawa, M. Sadakane, D. Buttrey, W. Ueda, An orthorhombic Mo_3VO_x catalyst most active for oxidative dehydrogenation of ethane among related complex metal oxides, Catal. Sci. Technol. 3 (2013) 380–387, https://doi.org/10.1039/C2CY20444D.
[10] E. Heracleous, A.F. Lee, K. Wilson, A.A. Lemonidou, Investigation of Ni-based alumina-supported catalysts for the oxidative dehydrogenation of ethane to ethylene: structural characterization and reactivity studies, J. Catal. 231 (2005) 159–171, https://doi.org/10.1016/j.jcat.2005.01.015.
[11] E. Heracleous, A.A. Lemonidou, Ni–Nb–O mixed oxides as highly active and selective catalysts for ethene production via ethane oxidative dehydrogenation. Part I: Characterization and catalytic performance, J. Catal. 237 (2006) 162–174, https://doi.org/10.1016/j.jcat.2005.11.002.
[12] P. Brussino, E.L. Mehring, M.A. Ulla, J.P. Bortolozzi, Tuning the properties of NiO supported on silicon-aluminum oxides: Influence of the silica amount in the ODH of ethane, Catal. Today (2021), https://doi.org/10.1016/j.cattod.2021.10.017. In Press.
[13] E. Moreno-Barrueta, C. Alvarado-Camacho, J.F. Durán-Pérez, A.-A. Morales-Pérez, C.O. Castillo, On the dynamics of the catalytic surface of a bimetallic mixed-oxide formulation during the oxidative dehydrogenation of ethane, Catal. Today (2021), https://doi.org/10.1016/j.cattod.2021.07.028. In Press.
[14] S.-B. Ivan, I. Fechete, F. Papa, I.-C. Marcu, Ethane oxydehydrogenation over TiP_2O_7-supported NiO catalysts, Catal. Today 366 (2021) 133–140, https://doi.org/10.1016/j.cattod.2020.02.005.
[15] J.L. Park, K.A. Canizales, M.D. Argyle, B.F. Woodfield, K.J. Stowers, The effects of doping alumina with silica in alumina-supported NiO catalysts for oxidative dehydrogenation of ethane, Microporous Mesoporous Mat 293 (2020) 109799, https://doi.org/10.1016/j.micromeso.2019.109799.
[16] P. Brussino, J.P. Bortolozzi, B. Dalla-Costa, E.D. Banús, M.A. Ulla, Double effect of La as a promoter for Ni/Al_2O_3 cordierite monoliths in the oxydehydrogenation of ethane (ODE), Appl. Catal. A: Gen 575 (2019) 1–10, https://doi.org/10.1016/j.apcata.2019.02.010.
[17] M.D. Irwin, D.B. Buchholz, A.W. Hains, R.P.H. Chang, T.J. Marks, *p*-Type semiconducting nickel oxide as an efficiency-enhancing anode interfacial layer in polymer bulk-heterojunction solar cells, PNAS 105 (2008) 2783–2787, https://doi.org/10.1073/pnas.0711990105.
[18] F. Trifiró, I. Pasquon, Classification of oxidation catalysts according to the type of metal-oxygen bond, J. Catal. 142 (1968) 412–416, https://doi.org/10.1016/0021-9517(68)90126-7.
[19] I. Popescu, Z. Skoufa, E. Heracleous, A.A. Lemonidou, I.-C. Marcu, A study by electrical conductivity measurements of the semiconductive and redox properties of Nb-doped NiO catalysts in correlation with the oxidative dehydrogenation of

ethane, Phys. Chem. Chem. Phys. 17 (2015) 8138–8147, https://doi.org/10.1039/C5CP00392J.
[20] B. Savova, S. Loridant, D. Filkova, J.M.M. Millet, Ni–Nb–O catalysts for ethane oxidative dehydrogenation, Appl. Catal., A 390 (2010) 148–157, https://doi.org/10.1016/j.apcata.2010.10.004.
[21] E. Heracleous, A.A. Lemonidou, Ni-Me-O mixed metal oxides for the effective oxidative dehydrogenation of ethane to ethylene - effect of promoting metal me, J. Catal. 270 (2010) 67–75, https://doi.org/10.1016/j.jcat.2009.12.004.
[22] M.O. Guerrero-Pérez, The fascinating effect of niobium as catalytic promoting agent, Catal. Today 354 (2020) 19–25, https://doi.org/10.1016/j.cattod.2019.04.008.
[23] P. Brussino, E.D. Banús, M.A. Ulla, J.P. Bortolozzi, NiO-based ceramic structured catalysts for ethylene production: Substrates and active sites, Catal. Today 383 (2022) 84–92, https://doi.org/10.1016/j.cattod.2020.09.005.
[24] C. Mateos-Pedrero, S. González-Carrazán, P. Ruiz, Preliminary results on the role of the deposition of small amounts of ZrO_2 on Al_2O_3 support on the partial oxidation of methane and ethane over Rh and Ni supported catalysts, Catal. Today 363 (2021) 111–121, https://doi.org/10.1016/j.cattod.2020.02.010.
[25] Y. Zhou, J. Lin, L. Li, M. Tian, X. Li, X. Pan, Y. Chen, X. Wang, Improving the selectivity of Ni-Al mixed oxides with isolated oxygen species for oxidative dehydrogenation of ethane with nitrous oxide, J. Catal. 377 (2019) 438–448, https://doi.org/10.1016/j.jcat.2019.07.050.
[26] M. Hurtado-Cotillo, D. Unsihuay, C.E. Santolalla-Vargas, A. Paredes-Doig, R. Sun-Kou, G. Picasso, Catalysts based on Ni-Fe oxides supported on γ-Al_2O_3 for the oxidative dehydrogenation of ethane, Catal. Today 366 (2020) 312–321, https://doi.org/10.1016/j.cattod.2019.05.044.
[27] B. Solsona, P. Concepcion, B. Demicol, S. Hernandez, J.J. Delgado, J.J. Calvino, J. M. López Nieto, Selective oxidative dehydrogenation of ethane over SnO_2-promoted NiO catalysts, J. Catal. 295 (2012) 104–114, https://doi.org/10.1016/j.jcat.2012.07.028.
[28] J.M. López Nieto, B. Solsona, R.K. Grasselli, P. Concepcion, Promoted NiO catalysts for the oxidative dehydrogenation of ethane, Top. Catal. 57 (2014) 1248–1255, https://doi.org/10.1007/s11244-014-0288-2.
[29] H. Zhu, D.C. Rosenfeld, D.H. Anjum, V. Caps, J.-M. Basset, Green synthesis of Ni–Nb oxide catalysts for low-temperature oxidative dehydrogenation of ethane, ChemSusChem 8 (2015) 1254–1263, https://doi.org/10.1002/cssc.201403181.
[30] H. Zhu, D.C. Rosenfeld, M. Harb, D.H. Anjum, M.N. Hedhili, S. Ould-Chikh, J.-M. Basset, Ni–M–O (M = Sn, Ti, W) catalysts prepared by a dry mixing method for oxidative dehydrogenation of ethane, ACS Catal. 6 (2016) 2852–2866, https://doi.org/10.1021/acscatal.6b00044.
[31] E. López, E. Heracleous, A.A. Lemonidou, D.O. Borio, Study of a multitubular fixed-bed reactor for ethylene production via ethane oxidative dehydrogenation, Chem. Eng. J. 145 (2008) 308–315, https://doi.org/10.1016/j.cej.2008.08.029.
[32] L. Kong, D. Li, Zh. Zhao, J. Li, L. Zhao, X. Fan, X. Xiao, Z., Xie, Preparation, characterization and catalytic performance of rod-like Ni–Nb–O catalysts for the oxidative dehydrogenation of ethane at low temperature, Catal. Sci. Technol. 9 (2019) 3416–3442, https://doi.org/10.1039/C9CY00519F.
[33] D. Delgado, R. Sanchís, J.A. Cecilia, E. Rodríguez-Castellón, A. Caballero, B. Solsona, J.M. López Nieto, Support effects on NiO-based catalysts for the oxidative dehydrogenation (ODH) of ethane, Catal. Today 333 (2019) 10–16, https://doi.org/10.1016/j.cattod.2018.07.010.
[34] J.L. Park, K.A. Canizales, M.D. Argyle, B.F. Woodfield, K.J. Stowers, The effects of doping alumina with silica in alumina-supported NiO catalysts for oxidative dehydrogenation of ethane, Microp, Mesop. Mat. 293 (2020), 109799, https://doi.org/10.1016/j.micromeso.2019.109799.
[35] P. Brussino, J.P. Bortolozzi, B.D. Costa, E.D. Banus, M.A. Ulla, Double effect of La as a promoter for Ni/Al_2O_3 cordierite monoliths in the oxydehydrogenation of ethane (ODE), Appl. Catal. A 575 (2019) 1–10, https://doi.org/10.1016/j.apcata.2019.02.010.
[36] E. Rodríguez-Castellón, D. Delgado, A. Dejoz, I. Vázquez, S. Agouram, J.A. Cecilia, B. Solsona, J.M. López Nieto, Enhanced NiO dispersion on a high surface area pillared heterostructure covered by niobium leads to optimal behaviour in the oxidative dehydrogenation of ethane, Chem. Eur. J. 26 (2020) 9371–9381, https://doi.org/10.1002/chem.202000832.
[37] F. Cavani, N. Ballarini, A. Cericola, Oxidative dehydrogenation of ethane and propane: How far from commercial implementation? Catal. Today 127 (2007) 113–131, https://doi.org/10.1016/j.cattod.2007.05.009.
[38] C.A. Gärtner, A. van Veen, J.A. Lercher, Oxidative dehydrogenation of ethane: common principles and mechanistic aspects, ChemCatChem 5 (2013) 3196–3217, https://doi.org/10.1002/cctc.201200966.
[39] I. Popescu, E. Heracleous, Z. Skoufa, A. Lemonidou, I.-C. Marcu, Study by electrical conductivity measurements of semiconductive and redox properties of M-doped NiO (M = Li, Mg, Al, Ga, Ti, Nb) catalysts for the oxidative dehydrogenation of ethane, Phys. Chem. Chem. Phys. 16 (2014) 4962–4970, https://doi.org/10.1039/C3CP54817A.
[40] D. Delgado, B. Solsona, R. Sanchıs, E. Rodríguez-Castellón, J.M. López Nieto, Oxidative dehydrogenation of ethane on diluted or promoted nickel oxide catalysts: influence of the promoter/diluter, Catal. Today 363 (2021) 27–35, https://doi.org/10.1016/j.cattod.2019.06.063.
[41] X. Zhao, M.D. Susman, J.D. Rimer, P. Bollini, Tuning selectivity in nickel oxide-catalyzed oxidative dehydrogenation of ethane through control over non-stoichiometric oxygen density, Catal. Sci. Technol. 11 (2021) 531–541, https://doi.org/10.1039/D0CY01732A.
[42] J. Li, R. Li, C. Wang, C. Huang, W. Weng, H. Wan, Oxidative dehydrogenation of ethane to ethylene over mesoporous Ni-based catalysts, Chin. J. Catal. 30 (2009) 714–716, https://doi.org/10.1016/S1872-2067(08)60122-9.
[43] J.T. Richardson, R. Scates, M.V. Twigg, X-ray diffraction study of nickel oxide reduction by hydrogen, Appl. Catal., A 246 (2003) 137–150, https://doi.org/10.1016/S0926-860X(02)00669-5.
[44] H. Zhu, H. Dong, P. Laveille, Y. Saih, V. Caps, J.-M. Basset, Metal oxides modified NiO catalysts for oxidative dehydrogenation of ethane to ethylene, Catal. Today 228 (2014) 58–64, https://doi.org/10.1016/j.cattod.2013.11.061.
[45] J. Santander, E. López, A. Diez, M. Dennehy, M. Pedernera, G. Tonetto, Ni–Nb mixed oxides: One-pot synthesis and catalytic activity for oxidative dehydrogenation of ethane, Chem. Eng. J. 255 (2014) 185–194, https://doi.org/10.1016/j.cej.2014.06.048.
[46] G. George, S. Anandhan, Synthesis and characterisation of nickel oxide nanofibre webs with alcohol sensing characteristics, RSC Adv. 4 (2014) 62009–62020, https://doi.org/10.1039/C4RA11083H.
[47] R.E. Dietz, G.I. Parisot, A.E. Meixner, Infrared absorption and raman scattering by two-magnon processes in NiO, Phys. Rev. B 4 (1971) 2302–2310, https://doi.org/10.1103/PhysRevB.4.2302.
[48] E. Aytan, B. Debnath, F. Kargar, Y. Barlas, M.M. Lacerda, J.X. Li, R.K. Lake, J. Shi, A.A. Balandin, Spin-phonon coupling in antiferromagnetic nickel oxide, Appl. Phys. Lett. 111 (2017) 252402, https://doi.org/10.1063/1.5009598.
[49] S. He, X. Zheng, L. Mo, W. Yu, H. Wang, Y. Luo, Characterization and catalytic properties of Ni/SiO_2 catalysts prepared with nickel citrate as precursor, Mater. Res. Bull. 49 (2014) 108–113, https://doi.org/10.1016/j.materresbull.2013.08.051.
[50] N. Mironova-Ulmane, A. Kuzmin, I. Steins, J. Grabis, I. Sildos, M. Pärs, Raman scattering in nanosized nickel oxide NiO, J. Phys. Conf. Ser. 93 (2007), 012039, https://doi.org/10.1088/1742-6596/93/1/012039.
[51] L. Smolakova, M. Kout, E. Koudelkova, L. Capek, Effect of calcination temperature on the structure and catalytic performance of the Ni/Al_2O_3 and Ni–Ce/Al_2O_3 catalysts in oxidative dehydrogenation of ethane, Ind. Eng. Chem. Res. 54 (2015) 12730–12740, https://doi.org/10.1021/acs.iecr.5b03425.
[52] J.S. Yoon, M.B. Park, Y. Kim, D.W. Hwang, H.-J. Chae, Effect of metal oxide–support interactions on ethylene oligomerization over nickel oxide/silica–alumina catalysts, Catalysts 9 (2019) 933, https://doi.org/10.3390/catal9110933.
[53] Y. Kathiraser, W. Thisartarn, K. Suttiumporn, S. Kawi, Inverse $NiAl_2O_4$ on $LaAlO_3$–Al_2O_3: unique catalytic structure for stable CO_2 reforming of methane, J. Phys. Chem. C 117 (2013) 8120–8130, https://doi.org/10.1021/jp401855x.
[54] Ch. Li, Y.-W. Chen, Temperature-programmed-reduction studies of nickel oxide/alumina catalysts: effects of the preparation method, Thermochim. Acta 256 (1995) 457–465, https://doi.org/10.1016/0040-6031(94)02177-P.
[55] B. Solsona, P. Concepción, J.M. López Nieto, A. Dejoz, J.A. Cecilia, S. Agouram, M. D. Soriano, V. Torres, J. Jiménez-Jiménez, E. Rodríguez Castellón, Nickel oxide supported on porous clay heterostructures as selective catalysts for the oxidative dehydrogenation of ethane, Catal. Sci. Technol. 6 (2016) 3419–3429, https://doi.org/10.1039/c5cy01811k.
[56] B. Mile, D. Stirling, M.A. Zammitt, A. Lovell, M. Webb, The location of nickel oxide and nickel in silica-supported catalysts: two forms of “NiO” and the assignment of temperature-programmed reduction profiles, J. Catal. 114 (1988) 217–229, https://doi.org/10.1016/0021-9517(88)90026-7.
[57] D. Delgado, B. Solsona, A. Ykrelef, A. Rodríguez-Gomez, A. Caballero, E. Rodríguez-Aguado, E. Rodríguez-Castellon, J.M. López Nieto, Redox and catalytic properties of promoted NiO catalysts for the oxidative dehydrogenation of ethane, J. Phys. Chem. C 121 (2017) 25132–25142, https://doi.org/10.1021/acs.jpcc.7b07066.
[58] V. Biju, Ni 2p X-ray photoelectron spectroscopy study of nanostructured nickel oxide, Mater. Res. Bull. 42 (2007) 791–796, https://doi.org/10.1016/j.materresbull.2006.10.009.
[59] M.A. van Veenendaal, G. Sawatzky, Nonlocal screening effects in 2p X-ray photoemission spectroscopy core-level line shapes of transition metal compounds, Phys. Rev. Lett. 70 (1993) 2459–2468, https://doi.org/10.1103/PhysRevLett.70.2459.
[60] B.P. Payne, M.C. Biesinger, N.S. McIntyre, Use of oxygen/nickel ratios in the XPS characterisation of oxide phases on nickel metal and nickel alloy surfaces, J. Electron Spectrosc. Relat. Phenom. 185 (2012) 159–166, https://doi.org/10.1016/j.elspec.2012.06.008.
[61] J.C. Dupin, D. Gonbeau, Ph. Vinatier, A. Levasseur, Systematic XPS studies of metal oxides, hydroxides and peroxides, Phys. Chem. Chem. Phys. 2 (2000) 1319–1324, https://doi.org/10.1039/A908800H.
[62] J. Haber, Mechanism of heterogeneous catalytic oxidation, in: R.A. Sheldon, R. S. van Santen (Eds.), Catalytic Oxidation: Principles and Applications, World Scientific, Singapore, 1995, pp. 17–51.
[63] D. Koushik, M. Jošt, A. Dučinskas, C. Burgess, V. Zardetto, C. Weijtens, M. A. Verheijen, W.M.M. Kessels, S. Albrecht, M. Creatore, Plasma-assisted atomic layer deposition of nickel oxide as hole transport layer for hybrid perovskite solar cells, J. Mater. Chem. C 7 (2019) 12532–12543, https://doi.org/10.1039/c9tc04282b.
[64] Y.E. Firat, A. Peksoz, Efficiency enhancement of electrochromic performance in NiO thin film via Cu doping for energy-saving potential, Electrochim. Acta 295 (2019) 645–654, https://doi.org/10.1016/j.electacta.2018.10.166.
[65] J.-W. Shia, Y. Zou, L. Cheng, D. Ma, D. Sun, S. Mao, L. Sun, Ch. He, Z. Wang, In-situ phosphating to synthesize Ni_2P decorated NiO/g-C_3N_4 p-n junction for enhanced photocatalytic hydrogen production, Chem. Eng. J. 378 (2019) 122161, https://doi.org/10.1016/j.cej.2019.122161.
[66] J. Zhang, J. Long, Z. Huang, J. Yan, X. Li, R. Dai, W. Sheng, L. Tan, Y. Chen, Obstructing interfacial reaction between NiOx and perovskite to enable efficient

and stable inverted perovskite solar cells, Chem. Eng. J. 426 (2021) 131357, https://doi.org/10.1016/j.cej.2021.131357.
[67] Zh. Lin, Du Ch, B. Yan, Ch. Wang, G. Yang, Two-dimensional amorphous NiO as a plasmonic photocatalyst for solar H_2 evolution, Nat. Commun. 9 (2018) 4036, https://doi.org/10.1038/s41467-018-06456-y.
[68] A. Bielanski, J. Haber, Oxygen in catalysis on transition Metal Oxides, Catal. Rev. Sci. Eng. 19 (1979) 1–41, https://doi.org/10.1080/03602457908065099.
[69] J.M. López, Nieto, B. Solsona, Gas phase heterogeneous partial oxidation reactions, in: J.C. Vedrine (Ed.), Metal Oxides in Heterogeneous Catalysis, Elsevier, Amsterdam, 2018, pp. 211–286.
[70] S.-B. Ivan, I. Popescu, I. Fechete, F. Garin, V.I. Pârvulescu, I.-C. Marcu, The effect of phosphorus on the catalytic performance of nickel oxide in ethane oxidative dehydrogenation, Catal. Sci. Technol. 6 (2016) 6953–6964, https://doi.org/10.1039/c6cy00946h.
[71] A.M. Turky, Electrical surface and catalytic properties of NiO as influenced by doping with CuO and Ag_2O, Appl. Catal., A 247 (2003) 83–93, https://doi.org/10.1016/S0926-860X(03)00089-9.
[72] Z. Skoufa, E. Heracleous, A.A. Lemonidou, On ethane ODH mechanism and nature of active sites over NiO-based catalysts via isotopic labeling and methanol sorption studies, J. Catal. 322 (2015) 118–129, https://doi.org/10.1016/j.jcat.2014.11.014.
[73] S. Agouram, A. Dejoz, F. Ivars, I. Vázquez, J.M. López Nieto, B. Solsona, Oxidative dehydrogenation of ethane: a study over the structure and robustness of Ni–W–O catalysts, Fuel Process. Technol. 119 (2014) 105–113, https://doi.org/10.1016/j.fuproc.2013.10.017.
[74] J. Estellé, P. Salagre, Y. Cesteros, M. Serra, F. Medina, J.E. Sueiras, Comparative study of the morphology and surface properties of nickel oxide prepared from different precursors, Solid State Ionics 156 (2003) 233–243, https://doi.org/10.1016/S0167-2738(02)00612-4.
[75] S. Rakshit, S. Chall, S.S. Mati, A. Roychowdhury, S.P. Moulik, S.Ch. Bhattacharya, Morphology control of nickel oxalate by soft chemistry and conversion to nickel oxide for application in photocatalysis, RSC Adv. 3 (2013) 6106–6116, https://doi.org/10.1039/c3ra21978j.